

FEASIBILITY ANALYSIS OF AN MHD INDUCTIVE GENERATOR COUPLED WITH A THERMOACOUSTIC RESONATOR

*A. Alemany*², *S. Carcangiu*¹, *R. Forcinetti*¹, *A. Montisci*¹, *J.P. Roux*³

¹ *DIEE, University of Cagliari, Piazza d'Armi, 09123 Cagliari, Italy*

² *SIMAP Laboratory, Domaine Universitaire, BP 75 38402 Saint Martin d'Hères, France*

³ *AREVA TA, CS50497, 13593 Aix-en-Provence Cedex 3, Toulouse, France*

This paper pertains to the feasibility analysis of a magnetohydrodynamic (MHD) inductive generator coupled with a Thermo Acoustic (TA) resonator. The MHD and TA processes have the great advantage to convert energy without mechanical moving components. In this work, first, the design criteria are given, then the order of magnitude of the obtained parameters is used to model the system by using the finite element method (FEM) to confirm the theoretical results. The conceptual idea and the FEM model are described.

Introduction. MHD power generation systems were originally investigated starting from the fact that the interaction of a plasma with a magnetic field must take place at much higher temperatures than could be obtained in a mechanical turbine. This kind of machines can only be efficient if the charges' concentration in the gas is at an adequate level. This is usually obtained by heating the gas until it reaches a high temperature and by seeding it with ionizing elements. In conventional MHD generators, a plasma passes through an intense magnetic field, so that, by closing the circuit on a load, the induced electromotive force determines an electric current in the fluid [1]. The main problems of the traditional MHD generators are the high temperatures necessary to ionize the gas and the high magnetic field (about 5 T) required to have significant outlet energy. The proposed device does not require an external magnetic field to work, on the contrary, it performs the energy conversion through the induction principle. The charge carriers are at a first stage created by means of an electrical discharge and then separated by an external, high voltage electrostatic field. Once the equilibrium is reached, if the gas inside the duct starts vibrating as a result of the TA phenomenon, the charge carriers give rise to an alternating electric current; this current induces an electromotive force in a toroidal coil wrapped around the duct and connected to the load. Thermoacoustic engines can convert high temperature heat into acoustic power with high efficiencies and without moving parts. They have a controlled mass and promise to be highly reliable. Coupling this system with an MHD generator will create an electric generator powered by the heat suitable for space applications [2–4].

The paper is organized as follows. In Section 1, the energy conversion process is qualitatively described. In Section 2, the results of a preliminary study are reported in order to propose a simplified theory about the performances of the generator and, therefore, to give the design criteria. Then a FEM analysis was performed to justify the assumptions of the design phase. In Section 3, the acoustic study of the gas is performed on the hypothesis of having a wave of pressure caused by the thermoacoustic effect; in Section 4, the electrostatic model is depicted and some results are reported. The last section provides some conclusions.

1. Energy conversion process. The TA phenomenon occurs when a great gradient of temperature is present in the longitudinal direction of a duct containing

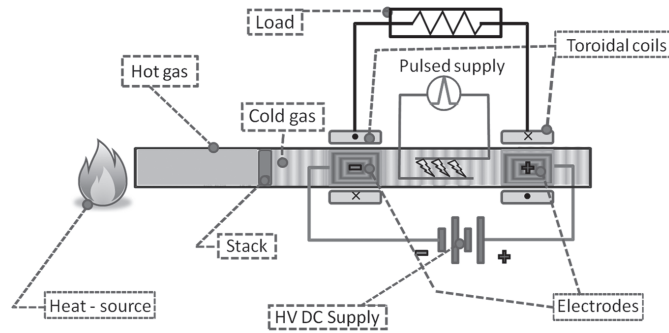


Fig. 1. Schematic view of the ionized MHD generator.

a gas. In order to obtain such gradient, we need a heat source and a stack inside the duct with a large surface. The TA effect allows to transform thermal energy into vibration energy. In this transformation, the gradient of temperature affects the flow rate of energy, whereas the frequency is determined by the length of the duct. The most important feature of TA is that there are no mechanical moving parts, and the working fluid is quasi static [5]. It represents a better solution with respect to the conventional MHD generators, because the flowing working fluid is substituted by a quasi-static gas, the external magnetic field by an electrostatic field, with a great simplification of the apparatus, and what is more, the electrodes for the retrieval of the generated current are no longer necessary.

The device proposed in this study (Fig. 1) includes two stages: the conversion of heat to mechanical energy of vibration at the first stage, and the conversion of such vibration to electrical energy. The working fluid is forced to become plasma by means of an electrical discharge caused by a pulsed high voltage generator connected to the gas by means of two electrodes inserted into the duct. Provided that the voltage pulse is high enough, the fact that the electric charge is generated by means of an electric discharge implies that the gas can be ionized also at low temperatures and seeding is not necessary. The charge carriers of opposite sign are separated by an external DC electric field applied to the gas by means of a proper capacitor. The voltage necessary to maintain in equilibrium the two clouds of charges of different sign depends linearly on the surface of the plates; that is the reason why the shape of such plates has to be chosen carefully.

Once the equilibrium is reached, if a wave of pressure travels along the duct because of the TA effect, the two clouds of charge carriers participate in the motion of the surrounding neutrals, giving rise to an alternating current. Such current induces an electromotive force in two toroidal coils wrapped around the duct in correspondence with the vibrating charges. The coils are connected to the electrical load, where the energy conversion process ends.

2. Theoretical development and device sizing. A first study has been done in order to perform a coarse sizing of the generator. Apart from the sign of the charges, the two clouds of charges give rise to the same phenomenon. For the sake of simplicity, let us to assume that the two toroidal coils are electrically independent. What follows can be independently referred both to the positive and to the negative charge carriers. The study starts from the Ampère equation and the equation of the circuit (Fig. 2):

$$2\pi R \cdot B(t) = \mu_t(I(t) - ni(t)). \quad (1)$$

In this expression, $I(t)$ is the total electric current in a cross-section generated

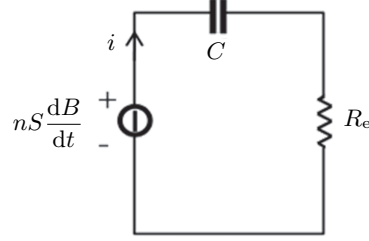


Fig. 2. Electric circuit scheme.

by the charge oscillation, $i(t)$ is the induced electric current in the toroidal coil, μ_f is the magnetic field of the core of the toroidal coil, where the magnetic induction $B(t)$ oscillates, and R is the mean radius of the toroidal ferromagnetic material. Two further contributions should be considered: the two electric fields of the armature reaction (see Eq. (9)), on the one hand, and of the charge distribution, on the other hand, generating the displacement currents. In this preliminary analysis we preferred to neglect such contributions. The induced current is controlled by the magnetic flux in the core of the cross-section S surrounded by n -turn coils. The electrical circuit of the coil comprises also the load resistance R_e and a capacitance C to compensate the self of the coil. We assume that the oscillation can be approximated by a sinusoid of frequency ω , therefore, the equations can be represented in the phasorial form. The equation of the electrical circuit reads as follows:

$$j\omega nS \cdot \mathbf{B} = \left(R_e + \frac{1}{j\omega C} \right) \cdot \mathbf{i} \Rightarrow B^2 = \frac{1}{\omega^2 n^2 S^2} \left(R_e^2 + \frac{1}{\omega^2 C^2} \right) \cdot i^2 \quad (2)$$

where $\mathbf{B} = B e^{j\phi}$ and $\mathbf{i} = i e^{j\psi}$. Let us call P_0 the required electrical power. Taking into account that $R_e = P_0/i^2$, we obtain

$$B^2 = \frac{1}{\omega^2 n^2 S^2} \left(\frac{P_0^2}{i^2} + \frac{i^2}{\omega^2 C^2} \right),$$

from which we can derive the condition for the minimum value of the induction field B ,

$$\frac{dB^2}{di^2} = \frac{1}{\omega^2 n^2 S^2} \left(-\frac{P_0^2}{i^4} + \frac{1}{\omega^2 C^2} \right) = 0. \quad (3)$$

Therefore, we can assess the value of the current circulating in the coil as being equal to the minimum of the magnetic induction: $i^2 = \omega C P_0$. Bearing in mind once again that $R_e = P_0/i^2$, that condition occurs when $R_e = 1/\omega C$.

Eq. (3) allows us to strongly reduce the complexity of the problem formulation and evidences that the minimum value of the magnetic induction occurs when the impedance of both the capacitor and the resistor have the same modulus:

$$-\omega nS \cdot \mathbf{B} = \frac{1}{\omega C} (1 + j) \cdot \mathbf{i} \Rightarrow \mathbf{i} = -\frac{\omega^2 nSC}{2} (1 - j) \cdot \mathbf{B}. \quad (4)$$

By considering the expression of the power

$$P_0 = R_e i^2 = i^2 / (\omega C),$$

we can obtain the value of the capacitance

$$C = 2P_0 / (\omega^3 n^2 S^2 B^2).$$

Such value of capacitance can be substituted into the Ampère equation. The phases are referred to the ionic current I . As a consequence, this current is represented by a real value. Eq. (1) becomes:

$$\left[\frac{2\pi R}{\mu_f} - \frac{P_0}{\omega S B^2} (1-j) \right] \cdot \mathbf{B} = \left[\frac{2\pi R}{\mu_f} \cdot B - \frac{P_0}{\omega S B} (1-j) \right] e^{j\phi} = I e^{j0} = \pi R_D^2 \sigma v_0, \quad (5)$$

where where R_D is the radius of the duct, σ is the average density of charge, v_0 is the amplitude of the sinusoidal velocity of charge carriers. This equation allows us to calculate the electric current in the gas so that the desired power and magnetic induction can be obtained. Due to the fact that the right-hand side of Eq. (5) is real, the phase of the term within brackets in the left-hand side has to be opposite to the exponential factor out of brackets. Thus, we obtain

$$\tan \phi = [2\pi R \omega S B^2 / \mu_f P_0 - 1]^{-1}. \quad (6)$$

We can calculate the value of B which is the modulus of \mathbf{B} , which corresponds to the minimum value of the ionic current I . To do that, we have to minimize the modulus of the term within brackets in Eq. (5) deriving

$$B^2 = \mu_f P_0 / (2\pi R \omega S). \quad (7)$$

This result comes up with an important consequence. In fact, by Eqs. (5) and (6) we derive the minimum of both B and I when the magnetic induction is in quadrature with respect to the gas current. By substituting Eq. (7) into Eq. (5) we obtain:

$$\pi R_D^2 \sigma v_0 = \sqrt{\frac{2\pi R P_0}{\mu_f \omega S}}. \quad (8)$$

Eqs. (7) and (8) allow us to perform the device sizing. For a given material of the torus core, Eq. (7) establishes a direct relationship between the required power, the size of the core and the frequency of the current. On the other hand, Eq. (8) provides indications on the size and on the operative conditions of the duct. As in the case of magnetic induction, the frequency and the cross-section of the core contribute to limiting this parameter, whereas the permeability and the radius of the torus result in having an opposite effect. Therefore, if we have heavy constraints on both magnetic induction and electric current in gas, it would be preferable to act on the frequency and cross-section of the torus.

Finally, in order to obtain the desired current I in the gas, we can see that the radius of the duct has a stronger effect with respect to both the density of charge and the velocity amplitude. These three parameters are constrained for different reasons. The radius of the duct affects the size of the device, so it could be critical in contexts, where this aspect is important, such as in aerospace applications. A high charge density will require high values of capacitance and voltage in order to separate positive from negative charges. The amplitude of the charges' velocity depends on the power injected into the system, then on the thermoacoustic resonator and the heat source.

The values of these parameters, reported in Table 1, represent the best compromise for a specific aerospace application. Changing the context, the best configuration of the parameters should be completely different.

By means of few substitutions we can obtain the current circulating in the coil:

$$\mathbf{i} = -\sqrt{\frac{2\pi R P_0}{\mu_f n^2 \omega S}} (1+j). \quad (9)$$

Table 1. Design parameters and results.

Real case scale		Demonstrative facility	
Design parameters	Results	Design parameters	Results
$P_0 = 200$ W	$i_0 = 1.6$ A	$P_0 = 10$ W	$i_0 = 0.252$ A
$R = 12$ cm	$V_{\text{coil}} = 177$ V	$R = 6$ cm	$V_{\text{coil}} = 56$ V
$R_D = 7$ cm	$I_0 = 11.28$ A	$R_D = 3.55$ cm	$I_0 = 1.78$ A
$\sigma = 15$ C/m ³	$U_0 = 17.72$ V	$\sigma = 15$ C/m ³	$U_0 = 5.61$ V
$v_0 = 30$ m/s	$R_e = 200$ Ω	$v_0 = 30$ m/s	$R_e = 10$ Ω
$n = 10$ tr	$C = 0.8$ μF	$n = 10$ tr	$C = 15.9$ μF
$S = 3 \cdot 10^{-3}$ m ²	$\Delta\phi = 37.9$ kV	$S = 3 \cdot 10^{-3}$ m ²	$\Delta\phi = 15.1$ kV
$\omega = 2\pi \cdot 10^3$ rad/s	$ B = 0.94$ T	$\omega = 2\pi \cdot 10^3$ rad/s	$ B = 0.297$ T
$\mu_f = 5\mu_0 \cdot 10^4$ H/m		$\mu_f = 5\mu_0 \cdot 10^4$ H/m	
$\delta = 0.5$ mm		$\delta = 0.5$ mm	
$\beta = 1000$		$\beta = 1000$	

By introducing in the Faraday's law the expressions of \mathbf{B} and \mathbf{i} from Eqs. (4) and (9), respectively, one obtains the voltage drop \mathbf{U} in the gas, which results to be in phase with the ionic current \mathbf{I} :

$$\mathbf{U} = \omega S \sqrt{\frac{\mu_f P_0}{2\pi R \omega S}} e^{j0}. \quad (10)$$

The voltage drop \mathbf{U} is due to the electric field generated by the alternated magnetic flux circulating in the core of the toroidal coil. Let us call this field *armature reaction*. It is possible to demonstrate [9] that the force lines of such electric field have the same shape of the magnetic field due to a turn of current circulating in the place of the magnetic flux. That electric field is always opposite to the velocity of the charge carriers that consequently are braked. The consequent difference in velocity between charge carriers and surrounding neutrals determines an expansion of the gas and the consequent loss of energy.

Finally, we can calculate the voltage E to be applied to the plates to maintain the charges in equilibrium in the gas:

$$C_D = \epsilon \frac{2\pi R_D L \beta}{\delta} = \frac{\pi R_D^2 L \sigma}{E} \Rightarrow E = \frac{\delta R_D}{2\epsilon \beta} \sigma = \frac{\delta I}{2\epsilon \beta \pi R_D v_0}, \quad (11)$$

where C_D is the capacitance of the plate+gas system, ϵ is the vacuum dielectric constant, L is the length of the plate, β is the ratio between the gas-plate interface surface A_D and the surface of the internal wall of the duct corresponding to the plate, δ is the mean distance between the cloud of charge carriers and the surface of the plate. It is worth specifying that in these calculations only the contribution of the convective electric current is taken into account, while the displacement currents, originating from the border effects of the electric field at the ends of the plates, are momentarily neglected.

To establish the order of magnitude, two sets of design parameters were used: the first one related to a real case scale and the second one to a demonstrative facility. The design parameters and the results are reported in Table 1.

3. Acoustic analysis. A first simulation was performed with the software COMSOL[®] in order to assess the bounds of the design parameters. To this end, we assumed that the MHD generator was coupled with a thermoacoustic resonator having a given frequency and power. Under this hypothesis, the velocity profiles

Table 2. Helium properties ($p = 50$ bar; $T = 293$ K).

Property	Value
Dynamic viscosity η [kg/m·s]	$1.9912 \cdot 10^{-5}$
Density ρ_0 [kg/m ³]	7.8
Heat capacity C_p [J/(kg·K)]	5195
Thermal conductivity k [W/(m·K)]	0.156
Prandtl number Pr	0.663

corresponding to the cross-section of the duct have been studied. Knowing the two-dimensional distribution of the velocities is mandatory to be sure that the charge carriers are involved in the vibrating motion. In fact, both the velocity and the charge density are non-uniformly distributed along the cross-section, therefore, if most charge carriers are concentrated in zones with null velocity, the conversion process cannot take place.

The device to be modelled is a glass tube containing helium (He), within which the propagation of the vibration occurs at a temperature of 293 K and a pressure of 50 bar.

As can be noticed from the previous study (Section 2), in order to optimize the performance of the device, the dimensionless parameter β has to be maximized. This parameter is the ratio between the surface of the actual capacitor plate and the surface of the wall of the corresponding segment of the duct. In order to have high values of β , we can use a plate constituted by a thick pack of layers having a very rough surface.

The formulation used for this study is referred to the thermoacoustic module of COMSOL[®]. Differently from what usually happens in acoustics (isentropic/lossless), this formulation takes into account the dissipative effects of viscous shear and heat conduction. These effects cannot be neglected in acoustic wave propagation through narrow geometries. Actually, thermal conduction and viscosity in the proximity of the duct walls become important because they create viscous and thermal boundary layers, where losses are significant [6]. The model is able to solve simultaneously the equations for the acoustic pressure p , the particle velocity vector \mathbf{u} , and the temperature T .

The length scale required to perform the thermoacoustic study results from the thickness of the viscous boundary layer

$$\delta_v = \frac{\eta}{\pi f \rho_0},$$

and the thickness of the thermal boundary layer

$$\delta_T = \frac{k}{\pi f \rho_0 C_p}$$

where η is the dynamic viscosity, ρ_0 is the equilibrium density, f is the frequency of the acoustic wave, k is the thermal conductivity, and C_p is the heat capacity.

Note that the thickness of both boundary layers decreases with increasing frequency f . The ratio of the two length scales is related to the non-dimensional Prandtl number Pr, which defines the relative importance of the thermal and viscous effects for a given material.

The properties of the gas are listed in Table 2 [7].

In order to simulate the thermoacoustic effect, a vibration with previously assigned values of amplitude and frequency was applied to the gas. In agreement

with the typical values from the literature [2], a value of 30 m/s for the velocity was chosen and consequently the inlet acoustic pressure was imposed. On the other hand, by assuming an ideal energy conversion process, the relative pressure at the outlet was set to zero, thus, also the outlet velocity resulted to be null.

Nevertheless, the usual layout of TA generators foresees at least two stacks acting at different points of the resonator, therefore, we can assume the hypothesis that the same process occurs near to both toroidal coils.

If, in order to increase β , a significant part of the cross-section is occupied by the grid, the viscous and thermal dissipative effects will beget high losses. This would cause a considerable reduction of the vibration velocity of the charge carriers thickened into this area.

On the other hand, in the literature, several numerical studies have highlighted the phenomenon of “dark space” [8] due to the formation of a strong potential along the wall causing the expulsion of the charge carriers. Due to this phenomenon, the charge density decreases rapidly in the proximity of the wall and becomes almost zero close to the wall. Consequently, the charges will not adhere exactly to the wall, but will thicken in a cloud that will remain at a certain distance from the plate; this phenomenon avoids the charge carriers to be thickened close to the boundary layers, where the dispersion is at its maximum due to the thermal and viscous effects.

The simulation was made with the following assumptions: a homogeneous medium, which means that the wavelength and the radius R_D of the tube must be large compared with the mean free path (this condition breaks down for $f > 10^8$ Hz and $R_D < 10^{-5}$ cm); no steady flow; small amplitude, sinusoidal perturbations (no circulation and no turbulence); the tube long enough, so that the end effects are negligible. The acoustic simulation solves a linearized, small parameter expansion of the Navier–Stokes equations, the momentum equation, the continuity equation, and the energy equation. In order to solve the viscous boundary layer, a very fine mesh near no-slip boundaries was considered (see Fig. 3).

The results of the acoustic analysis are reported hereunder. The velocity profile in the axial direction in the cross-section of a rigid cylinder is completely determined by the shear wave number $s = R_D \sqrt{(\rho_0 \cdot \omega) / \eta}$. Given the gas with a

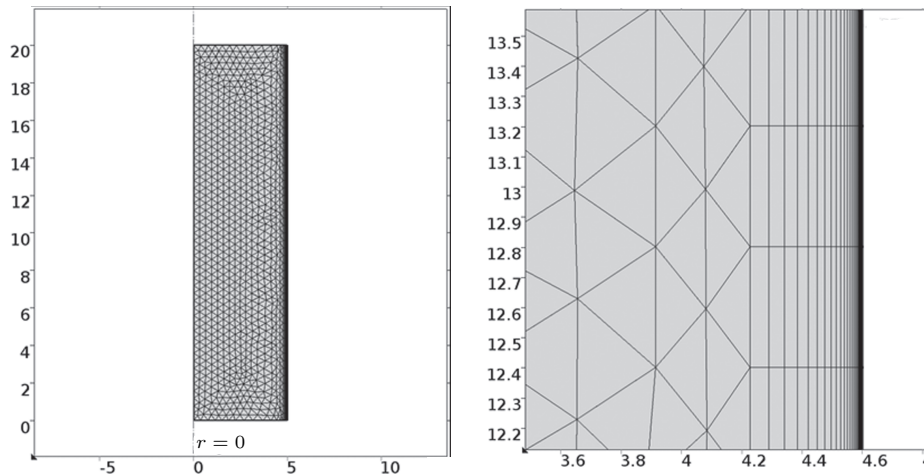


Fig. 3. Meshed model with boundary layer detail.

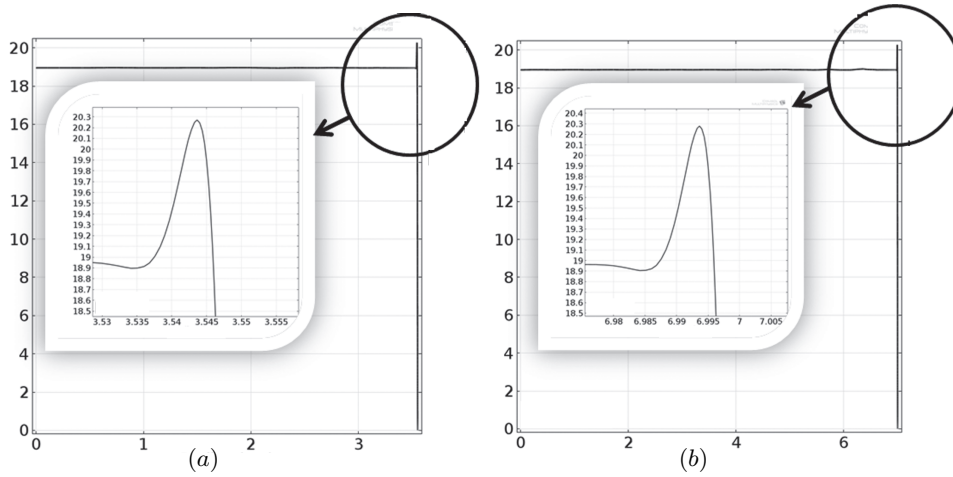


Fig. 4. Velocity distribution in the axial direction for the duct with (a) $R_D = 3.55$ cm and (b) $R_D = 7$ cm ($f = 1$ kHz).

set pressure (see Table 2), the parameters, affecting the velocity distribution, are mainly the working frequency and the radius of the duct.

Different velocity distributions and the corresponding shear wave number have been obtained with a parametric study by setting the radius of the duct equal to 0.1 cm, 1 cm, 1.5 cm, 2 cm, 3.55 cm (radius relative to demonstrative facility), 5 cm and 7 cm (radius relative to real device), and by varying the frequency from 10^{-2} Hz to 10^3 Hz. In Fig. 4, the velocity distributions at the working frequency ($f = 1$ kHz) for the demonstrative facility ($R_D = 3.55$ cm) and for the real device ($R_D = 7$ cm) are reported. In the same figure, an enlargement shows in details the velocity profile in the proximity of the wall. In both cases, the velocity profiles have the same shape with small peaks close to the wall.

The obtained results confirm the theoretical ones (Fig. 5) [6]. In fact, at low values of the shear wave number ($0.4 < s < 4$) the axial velocity shows a parabolic profile. At higher values ($s > 4$), the amplitudes of the velocity in the center of the tube become smaller and the profile becomes more and more uniform. With very high values of the shear wave number, the velocity profile is almost completely flat, with small peaks close to the tube wall.

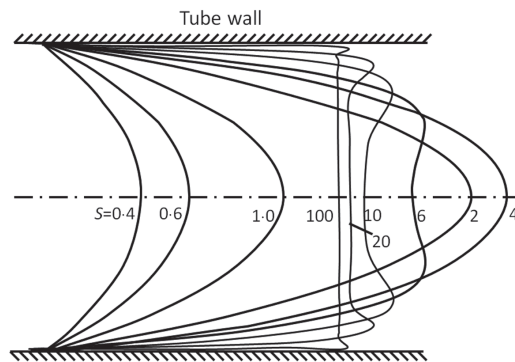


Fig. 5. Theoretical velocity distribution in the axial direction by varying the shear wave number [6].

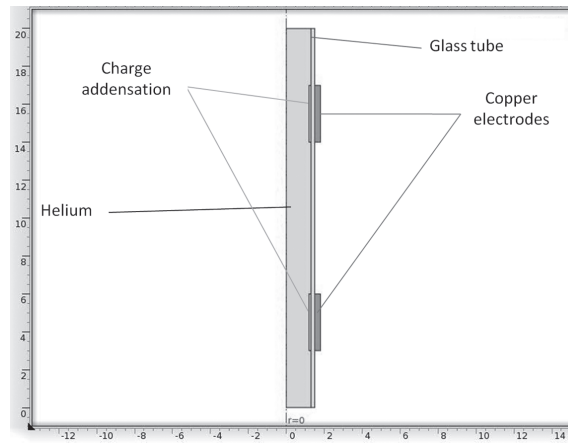


Fig. 6. 2D axisymmetric model geometry.

4. Electrostatic analysis. Another simulation was performed to study the electrostatic behavior of the generator. The model geometry (see Fig. 6) consists of a glass tube closed at the ends containing ionized helium gas with the properties summarized in Table 2. Two copper sleeve plates were positioned at an equal distance from the duct extremities and it was assumed that they were connected to a HVDC power supply. In that case, the ratio β between the surface of the plate and the surface of the wall (see Eq. (11)) was equal to unity. The electric potential E represents the dependent variable of the problem. A space charge density σ (see Table 1) was inserted near the sleeves as a result of a previous charge separation.

With a parametric analysis, by varying the external source HVDC in a range from 1 MV to 2 MV (Fig. 7a), an optimal value of voltage equal to 1.63 MV was found (Fig. 7b). Applying this value to the copper plates, the electric potential profile was null and flat in the central zone between the two plates (Fig. 7b), where the electrical field was thus equal to zero. As shown in Fig. 8a, the electric field

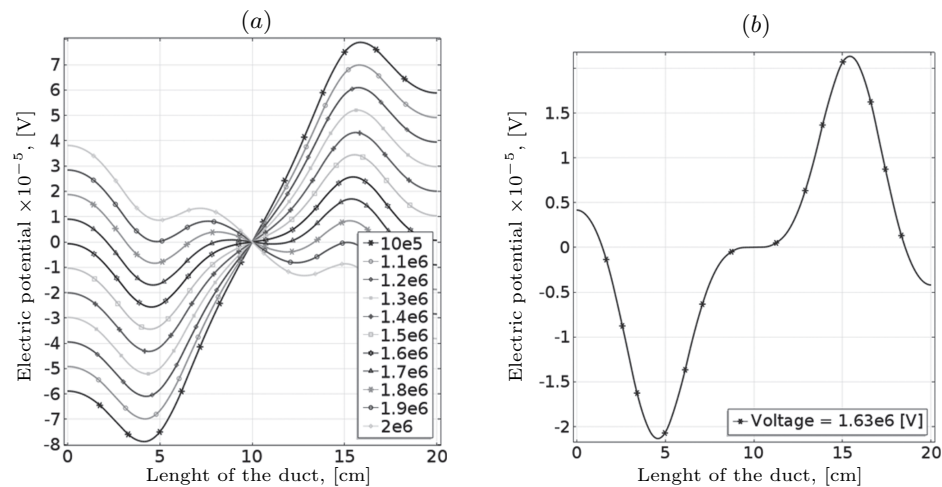


Fig. 7. (a) Parametric (voltage from 1 MV to 2 MV) and (b) optimal ($V = 1.63$ MV) distribution of the electrical potential along the duct.

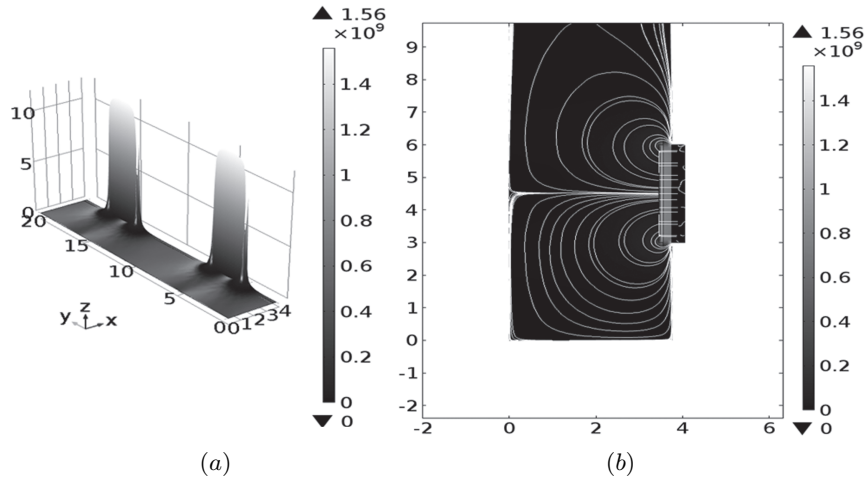


Fig. 8. Electric field along the duct ($V = 1.63$ MV): (a) mapping and (b) force lines.

is mainly confined in the inner volume within each sleeve. This allows to achieve an equilibrium condition for the charge distributions that the electric field cannot alter.

The value of the needed voltage can be reduced by increasing the plate surface, for example, by using a pack of layers, as described above ($\beta \gg 1$). Therefore, by assuming $\beta = 1000$, like in Table 1, the voltage we need is reduced to 1.63 kV. This value differs by one order of magnitude from the theoretical one because we suggest two different charge distributions.

Finally, the force lines of the electric field along the duct are shown in Fig. 8b.

5. Conclusions. In this work, a numerical study of an inductive MHD generator exploiting the thermoacoustic effect has been presented.

The proposed device aims to overcome the typical drawbacks of the conventional MHD generators, such as the need to operate at high temperatures and to have superconducting coils for the generation of the external magnetic field.

The analysis was subdivided into a theoretical part and a simulation part. Firstly, the design criteria were given to state in a first approximation the parameters of the generator for a given set of requirements. Subsequently, the results of FEM analysis that justify the assumptions of the design phase were reported. The parametric analysis furnished useful preliminary results about the feasibility of the system and its performance.

REFERENCES

- [1] R.J. ROSA. *Magnetohydrodynamic Energy Conversion* (Hemisphere Publishing, Washington, D.C. 1987).
- [2] A. ALEMANY, A. KRAUZE, AND M. AL RADI. Thermo acoustic – MHD electrical generator. *Energy Procedia*, vol. 6 (2011), pp. 92–100.
- [3] S. BACKHAUS, E. TWARD, AND M. PETACH. Thermoacoustic power systems for space applications. In: *AIP Conference Proceedings*, vol. 608 (2002) , pp. 939–944.

- [4] S. BACKHAUS, E. TWARD, AND M. PETACH. Traveling-wave thermoacoustic electric generator. *Applied Physics Letters*, vol. 85 (2004), no. 6, pp. 1085–1087.
- [5] G.V. SWIFT. *Thermoacoustic energy conversion. Handbook of Acoustics* (Springer, New York, 2007), pp. 239–254.
- [6] H. TIJDEMAN. On the propagation of sound waves in cylindrical tubes. *Journal of Sound and Vibration*, vol. 39 (1975), pp. 1–33.
- [7] H. PETERSEN. *The Properties of Helium* (Danish Atomic Energy Commission, Report No. 224, 1970.)
- [8] S. ROY, AND D.V. GAITONDE. Ionized collisional flow model for atmospheric RF application. *Proc. the 35th AIAA Plasmadynamics and Lasers Conference* (Portland, OR, 2004).
- [9] S. CARCANGIU, AND A. MONTISCI. Assessment of the machine parameters affecting the overall performance of an inductive MHD generator. *Proc. 2012 IEEE International Energy Conference and Exhibition, ENERGYCON 2012* (Florence, Italy, 2012).

Received 13.01.2015